InSAR datum connection using GNSS-augmented radar transponders

Mahapatra, Pooja; van der Marel, Hans; van Leijen, Freek; Samiei Esfahany, Sami; Klees, Roland; Hanssen, Ramon

DOI
10.1007/s00190-017-1041-y

Publication date
2017

Document Version
Final published version

Published in
Journal of Geodesy

J Geod
DOI 10.1007/s00190-017-1041-y

ORIGINAL ARTICLE

InSAR datum connection using GNSS-augmented radar transponders

Pooja Mahapatra[1] · **Hans van der Marel**[1] · **Freek van Leijen**[1] · **Sami Samiei-Esfahany**[1] · **Roland Klees**[1] · **Ramon Hanssen**[1]

Received: 27 February 2017 / Accepted: 25 May 2017

Abstract Deformation estimates from Interferometric Synthetic Aperture Radar (InSAR) are relative: they form a 'free' network referred to an arbitrary datum, e.g. by assuming a reference point in the image to be stable. However, some applications require 'absolute' InSAR estimates, i.e. expressed in a well-defined terrestrial reference frame, e.g. to compare InSAR results with those of other techniques. We propose a methodology based on collocated InSAR and Global Navigation Satellite System (GNSS) measurements, achieved by rigidly attaching phase-stable millimetre-precision compact active radar transponders to GNSS antennas. We demonstrate this concept through a simulated example and practical case studies in the Netherlands.

Keywords InSAR · Transponder · Radar · Deformation · GNSS · GPS · Datum connection · Terrestrial Reference Frame

1 Introduction

Interferometric Synthetic Aperture Radar (InSAR) is used to estimate double-difference displacements (in space and in time) between radar scatterers, based on their complex-valued reflections. These estimates are inherently relative—they form a *free* network, i.e. not defined in a geodetic datum, as the motion of points can only be observed in a relative way (Huygens 1646; Stevens 1946). For a free network, an arbitrary local datum is usually chosen, to a reference epoch ('master' time), and to a reference point (or the average of scatterers within a reference area) within the image. Often, a convenient deterministic value is chosen, e.g. zero displacement assuming that the reference point is situated in a stable area. Therefore, the interpretation of all displacement results is subject to this assumption, which may not be true in reality. Large-scale motion, affecting the entire area of interest including the reference point in the same way, is undetectable, while local motion affecting only the reference point would propagate to the deformation estimates of all other points.

Such a free network makes it impossible to relate InSAR deformation estimates with other datasets, e.g. leveling data or sea-level change. Whenever two or more sets of estimates stem from specific reference frames, or *datums*, there is a need for *datum connection* (Rummel and Teunissen 1988). In this paper, we propose a datum connection method to precisely convert the deformation results of InSAR surveys from a local reference frame to a standard Terrestrial Reference Frame (TRF), with the associated noise variance–covariance matrices. In the remainder of this paper, we use the term 'absolute' displacement to mean displacement expressed in a well-defined TRF.

Taking the example of Persistent Scatterer (PS) InSAR, techniques such as GNSS have been used in several studies to confirm PS displacement estimates and/or perform joint inversion, e.g. Bock et al. (2012), Bürgmann et al. (2006), Delouis et al. (2002), Hu et al. (2016), Pritchard et al. (2002), Tosi et al. (2016) and Zhu et al. (2015). These studies make use of existing natural PS within a reference area (i.e. a certain radius from a GNSS station), assuming that these PS measure the same kinematic signal as the GNSS antenna. However, such PS are not guaranteed to exist, especially in rural areas. Moreover, it is unlikely that a PS located near (but not rigidly connected to) a GNSS antenna shows identical displacement as that measured by the antenna. The differences may arise due to different measurement inaccuracies, as well

✉ Pooja Mahapatra
pooja.mahapatra@gmail.com

[1] Delft University of Technology, Delft, The Netherlands

Published online: 15 June 2017

as the presence of local variations as shown in Ketelaar and Hanssen (2003) and Ketelaar (2008). Sometimes, even two different parts of the same building may deform differently (Adam et al. 2009; Chang and Hanssen 2014; Gernhardt et al. 2010; Reale et al. 2011; Zhu and Bamler 2010a, b; Zhu and Shahzad 2014). In order to perform a rigorous datum connection between InSAR and GNSS, it is important to know the location of the effective scattering phase centre of the PS reference, and ensure that there is no relative displacement between this phase centre and the GNSS antenna. This is most easily and precisely done by attaching artificial PS devices such as corner reflectors or active transponders to the GNSS antenna.

For precise InSAR datum connection at the global scale, a solution is desired where the PS reference points can be attached rigidly to GNSS antennas that form part of the continuously-operating International GNSS Service (IGS) network (International GNSS Service 2016; Dow et al. 2009). GNSS antennas have been collocated[1] with corner reflectors in the past, to derive the precision of InSAR measurements, e.g. Ferretti et al. (2007) and Marinkovic et al. (2007). Some advantages of using corner reflectors as coherent targets are that they are conceptually simple and can be constructed economically. They do not require a source of power and do not possess electronic components whose performance could decay/drift over time. However, they also suffer from a few drawbacks. Corner reflectors (e.g. for C- and L-bands) are large and heavy, and their shape and material properties make it difficult to rigidly attach them to permanent GNSS antennas without causing disturbances to the GNSS time-series (e.g. due to loading or multipath effects). For long-term deployment spanning several years, these large structures can be disturbed or geometrically altered by weather/thermal conditions or fauna. They require protection from the accumulation of snow, rain and general debris, and/or need periodic maintenance. Using the same corner reflector structure for different satellites and looking directions (orbital passes and beam modes) would also entail heavier/more complicated designs, and/or moving parts.

Here we propose a novel approach for precise datum connection. Small and lightweight PS such as *compact active transponders* (CATs) (Fromberg 2014; Mahapatra et al. 2014; Mahapatra 2015) are installed and used as InSAR reference points. Their phase stability has been shown in Mahapatra et al. (2014) and Mahapatra (2015) to be comparable to that of corner reflectors up to a few millimetres. Each transponder is rigidly attached to a GNSS antenna; the displacement of the InSAR reference point is therefore precisely measured through GNSS in a standard TRF. This measurement is stochastic, and the errors can be propagated. The location of the phase centre of the transponder is known (Fromberg 2014; Mahapatra 2015) to be within the small plastic transponder box, and the sturdy connection between the transponder and the GNSS antenna ensures that both of them experience identical displacements.

Transponders are sealed compact units that are lightweight (<4 kg) and inconspicuous. They function autonomously with internal power for more than a year and are not susceptible to environmental impact such as strong winds, precipitation and debris accumulation. They require maintenance to the extent that visits may be required to change/charge the battery and check for clock drift, or upload a new SAR acquisition schedule if needed. Since a transponder is transmitter-specific and only turned on at the time of the satellite overpass, it offers little interference to other radar or radio targets. Transponders can be used for both ascending and descending satellite modes in a single fixed setup, providing two components of motion vector as well as doubling the frequency of measurements. Since the signal frequency can be pre-programmed, they can be used for various (C-band) SAR sensors in a single setup. Advanced transponders may also be equipped with additional features such as signal encoding, which can be used to decouple the transponder signal from the background signal, e.g. Waegel et al. (1999).

A limitation of current transponders is battery maintenance: the battery needs to be recharged once in several months, and may eventually need replacement if deployed over several years. This may be circumvented by the use of external power sources such as solar panels, or connecting to the power supply of the GNSS antenna that the transponder is physically attached to. Additionally, transponders are more difficult to manufacture in compact sizes at higher frequencies (e.g. X-band); for such frequencies, corner reflectors of comparable sizes can be constructed. Finally, the operational use of transponders may require transmission licences, which vary across national boundaries. Despite these aspects, transponders can be a practical alternative to corner reflectors, particularly for C-band InSAR.

In the following sections, we describe the approach for connecting InSAR to a TRF, and experimental results with GNSS-augmented radar transponders. We begin with a mathematical framework in Sect. 2. The theory behind datum connection based on classical geodetic principles using a simulated InSAR example as an illustration is described in Sect. 3. The experimental setup and results of the proposed method using Radarsat-2 data at IJmuiden, the Netherlands, where InSAR and GNSS measurements are collocated at a tide-gauge, are discussed in Sect. 4. 'Absolute' InSAR displacement results are also presented, along with a description of the various factors to be considered for precise datum connection. In Sect. 5, additional experiments at Eijsden and Vlissingen are described, and a collocation feasibility map of all the permanent GNSS stations in the Netherlands is

[1] Used in this context to mean physically connected at the same location, unrelated to statistical collocation.

determined. Finally, Sect. 6 provides a discussion and some recommendations.

2 Mathematical framework

Mathematically, the InSAR-derived double-difference deformation at location $p_1(x_1, y_1)$ and (slave) time t_1, with respect to reference location $p_0(x_0, y_0)$ and reference (master) time t_0, is given by

$$\Delta_p \Delta_t h = [h(p_1, t_1) - h(p_1, t_0)] - [h(p_0, t_1) - h(p_0, t_0)] \tag{1}$$

where h denotes the unit vector in an arbitrary direction. Often using the vertical direction is most convenient, but line-of-sight (LoS) direction may be used as well. $h(p_0, t_1)$ can be rewritten as

$$h(p_0, t_1) = h(p_0, t_0) + v(p_0) \times (t_1 - t_0) \tag{2}$$

where $v(p_0)$ is the velocity of the reference point, assuming linear displacement between master and slave acquisitions. Our quantity of interest is $[h(p_1, t_1) - h(p_1, t_0)]$, which is the deformation of point p between epochs t_1 and t_0. Using Eq. (2) in Eq. (1), we get

$$[h(p_1, t_1) - h(p_1, t_0)] = \Delta_p \Delta_t h + v(p_0) \times (t_1 - t_0). \tag{3}$$

The 'absolute' deformation can therefore be estimated from the double-difference value $\Delta_p \Delta_t h$ which is estimated from InSAR, in combination with the velocity of the reference point $v(p_0)$.

The term $v(p_0)$ is often postulated (e.g. by assuming the local stability of well-founded buildings), and is therefore considered deterministic. Such an approach is subjective, and quality assessment or control is difficult. Instead, $v(p_0)$ can be estimated by connecting the InSAR reference point to collocated geodetic measurements, e.g. a GNSS antenna capable of precise three-dimensional positioning. The reference point displacement and height (in a standard TRF) are then stochastic, and the associated errors can be propagated. All the other InSAR-derived displacements can subsequently be defined in the same TRF.

2.1 *S*-transformations

InSAR phase observations and derived displacement estimates are stochastic, with a precision that can be described completely by their variance–covariance matrix (VCM) e.g. Agram and Simons (2015), Hanssen (2001, 2004), Kampes (2006), Ketelaar (2008), Leijen (2014) and Liu (2012). Considering the persistent scatterer (PS) approach Ferretti et al. (2001), Hooper (2006), Kampes (2006), Leijen (2014) and Usai and Hanssen (1997), PS that are closer to the reference point have smaller variances than those farther away (owing to e.g. spatially-correlated atmospheric errors), making the VCM of PS displacements depend on the choice of the reference point.

The theory of *similarity-* or *S-transformations* (Baarda 1981; Kuang 1996; Strang and Borre 1997; Teunissen 1985) can be used to transform displacement estimates from one datum to another, and to give the relation between VCMs arising from the choice of different reference points. If $\underline{y}_1$ is the vector of displacements (length m) defined in a reference system or datum D_1, and $\underline{y}_2$ the vector of the same observations but defined in another datum D_2, the transformation from $\underline{y}_1$ to $\underline{y}_2$ can be represented by a linear transformation S as

$$\underline{y}_2 = S\underline{y}_1, \tag{4}$$

and the associated quality of the observations, denoted by the VCMs Q_{y_1} and Q_{y_2} respectively, can be propagated as

$$Q_{y_2} = S Q_{y_1} S^{\mathrm{T}}. \tag{5}$$

The generic form of S, called the S-transformation matrix, is given by Baarda (1981), Kuang (1996), Strang and Borre (1997) and Teunissen (1985)

$$S = I - H(D_2^{\mathrm{T}} H)^{-1} D_2^{\mathrm{T}} \tag{6}$$

with I being an $m \times m$ identity matrix. D_i is a matrix that defines the datum in each case i, i.e.

$$D_1^{\mathrm{T}} \underline{y}_1 = 0 \text{ and } D_2^{\mathrm{T}} \underline{y}_2 = 0 \tag{7}$$

for the two datums, respectively.

For the one-dimensional displacement monitoring case of InSAR (only in vertical or LoS direction), D_i is a binary unit vector at the location(s) of the reference point(s). As an example, if the displacement at the kth location is assigned as the transformed reference point, then $D_2 = [0\ 0\ \ldots\ 1\ldots\ 0]^{\mathrm{T}}$, with the value of unity at the kth position. The vector H is a basis for the null space (Teunissen 1985), derived from the inner constraint of the measurement network according to which the average displacement is set to zero (Baarda 1981; Kuang 1996; Teunissen 1985). Such a constraint is necessary to set the datum of a free network. In other words, H is the most generic case of D_i where the average of all displacements is taken as reference, i.e. $H = [1\ 1\ \ldots\ 1\ldots\ 1]^{\mathrm{T}}$. We proceed to apply this theory to InSAR-GNSS datum connection in the following section.

3 Datum connection for InSAR

In this section, we delve into the theory behind datum connection based on classical geodetic principles, using a simulated InSAR example as an illustration.

3.1 PS-GNSS collocation

In order to connect InSAR to the GNSS datum, it is required that the InSAR reference point and the corresponding GNSS benchmark reflect the same kinematic signal. A stable radar scatterer (i.e. a PS) such as a transponder (Fromberg 2014; Mahapatra et al. 2014; Mahapatra 2015) is physically connected to a GNSS antenna as shown in Fig. 1, ensuring that they experience the same displacements.

3.2 'Absolute' InSAR displacement estimates

Consider a simulated scenario of cumulative vertical displacements with respect to the InSAR master time epoch, as shown in the PS deformation map of Fig. 2a. The reference PS and the GNSS antenna are marked with a circle and a cross, respectively; note that the GNSS antenna is not collocated with a PS measurement. The associated VCM of the displacement estimates is shown in Fig. 2e, with the PS sorted in the order of increasing distance from the GNSS antenna. The GNSS antenna has a collocated PS (transponder) with double-difference measurement precision taken to be 1 mm (a reasonable estimate, as shown in Mahapatra (2015) for Radarsat-2 data).

We proceed to connect the PS results to the GNSS datum as follows:

1. The PS results $\underline{y}_{\text{initial}}$ with the initial reference point are first transformed to another datum D_{trans} defined by the transponder (Fig. 2b). Using the notation of Eqs. (5)–(7),

$$S_{\text{trans}} = I - H(D_{\text{trans}}^{\text{T}} H)^{-1} D_{\text{trans}}^{\text{T}} \tag{8}$$

$$\underline{y}_{\text{trans}} = S_{\text{trans}} \underline{y}_{\text{initial}} \tag{9}$$

setting the unity value in D_{trans} at the location corresponding to the transponder. The quality of displacement estimates is propagated to the VCM shown in Fig. 2f by

$$Q_{y_{\text{trans}}} = S_{\text{trans}} Q_{y_{\text{initial}}} S_{\text{trans}}^{\text{T}}. \tag{10}$$

2. The transformed PS results $\underline{y}_{\text{trans}}$ are then connected to a standard TRF, by adding the GNSS measurement to all the PS and propagating the errors of both techniques, i.e.

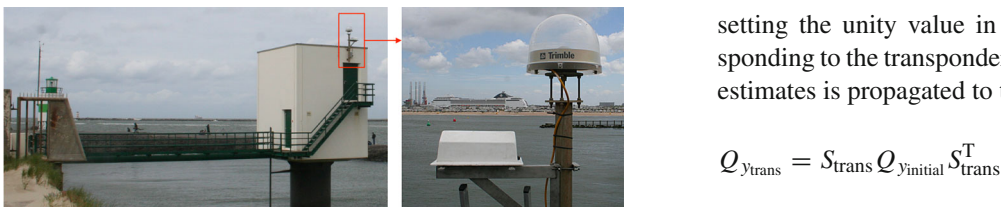

Fig. 1 Example of a collocated transponder-GNSS installation at a tide-gauge in IJmuiden, the Netherlands

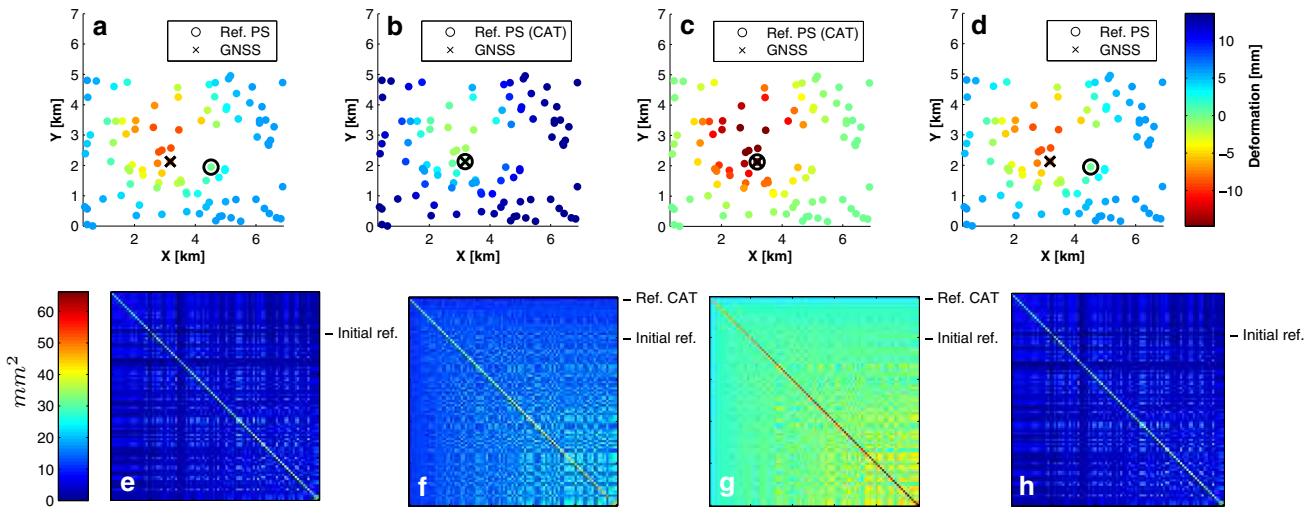

Fig. 2 **a** PS deformation map with respect to the initial reference point ($\underline{y}_{\text{initial}}$). **b** PS deformation map with respect to the reference transponder, transformed from (**a**), without connecting to GNSS datum ($\underline{y}_{\text{trans}}$). **c** PS deformation map with respect to reference transponder, transformed from (**b**), after connecting to GNSS datum ($\underline{y}_{\text{TRF}}$). This shows the 'absolute' displacement of every point, including the reference point, since the InSAR master time epoch. **d** PS map again with respect to the initial reference point ($\hat{\underline{y}}_{\text{initial}}$), transformed back from (**c**). **e**–**h** VCMs ($Q_{y_{\text{initial}}}$, $Q_{y_{\text{trans}}}$, $Q_{y_{\text{TRF}}}$ and $Q_{\hat{y}_{\text{trans}}}$) corresponding to **a**–**d**. PS points have been sorted in the order of increasing distance from the GNSS station in the VCMs. **a**, **d**, and their qualities (**e**, **h**), are identical

$$\underline{y}_{\mathrm{TRF}} = \underline{y}_{\mathrm{trans}} + H\underline{y}_{\mathrm{GNSS}} \tag{11}$$

where $\underline{y}_{\mathrm{GNSS}}$ is the GNSS measurement which can be linked to a standard TRF. In this example, $\underline{y}_{\mathrm{GNSS}}$ is assumed to be a subsidence value of 13.5 mm with respect to the GNSS measurement acquired at the InSAR master time epoch. Linear least-squares error propagation yields

$$Q_{y\mathrm{TRF}} = Q_{y\mathrm{trans}} + HQ_{y\mathrm{GNSS}}H^{\mathrm{T}} \tag{12}$$

where $Q_{y\mathrm{GNSS}}$ contains the variance of the GNSS measurement, taken to be 16 mm^2 in this example. Fig. 2c, g show the PS map connected to the GNSS datum and the associated quality, respectively. This PS map shows the 'absolute' displacement of every point, including the reference point.

It can be shown analytically that the double-difference information content in all the datums (Fig. 2e–g) is identical, irrespective of the GNSS measurements and their quality. Let $\underline{y}_{\mathrm{initial}}$ and $\underline{\hat{y}}_{\mathrm{initial}}$ denote, respectively, the original double-difference InSAR survey results with respect to the initial reference point, and the results transformed back to the initial reference point after GNSS datum connection. To show that $\underline{\hat{y}}_{\mathrm{initial}} = \underline{y}_{\mathrm{initial}}$, we make use of the following properties of S-transformations for any two datums D_1 and D_2 (Teunissen 1985):

1. $S_1\underline{y}_1 = \underline{y}_1$: measurements transformed to their own datum remain the same.
2. $S_1S_1 = S_1$: transforming to the same datum twice is equivalent to doing so only once.
3. $S_1S_2 = S_1$: transforming to a datum via another datum is equivalent to directly transforming to the final datum.

Using Eq. (4) and the equations in Sect. 3, the back-transformed set of measurements are given by

$$\underline{\hat{y}}_{\mathrm{initial}} = S_{\mathrm{initial}}\underline{y}_{\mathrm{TRF}} \tag{13}$$

$$= S_{\mathrm{initial}}(S_{\mathrm{trans}}\underline{y}_{\mathrm{initial}} + H\underline{y}_{\mathrm{GNSS}}) \tag{14}$$

From properties (1) and (3), $S_{\mathrm{initial}}S_{\mathrm{trans}}\underline{y}_{\mathrm{initial}} = \underline{y}_{\mathrm{initial}}$. By expanding S_{initial} using Eq. (6),

$$\underline{\hat{y}}_{\mathrm{initial}} = \underline{y}_{\mathrm{initial}} + [H - H(D_{\mathrm{initial}}^{\mathrm{T}}H)^{-1}(D_{\mathrm{initial}}^{\mathrm{T}}H)]\underline{y}_{\mathrm{GNSS}} \tag{15}$$

$$= \underline{y}_{\mathrm{initial}} \tag{16}$$

which also implies that

$$Q_{\hat{y}_{\mathrm{initial}}} = Q_{y_{\mathrm{initial}}}. \tag{17}$$

This is visualized in Fig. 2d, h, where transforming $\underline{y}_{\mathrm{TRF}}$ back to the initial reference system gives results identical to Fig. 2a, e. In other words, double-difference information is preserved during datum transformation and connection, irrespective of the transponder and GNSS measurements and quality. The added value of the proposed methodology is that these spatially-relative displacements can be converted into 'absolute' height changes with respect to a TRF. The VCM of these 'absolute' heights then also includes the quality of GNSS measurements.

The simplified scenario described in this section can be extended to time-series displacements incorporating temporal variance-covariance information, as well as to multi-track and multi-GNSS cases.

4 The IJmuiden experiment

A compact active radar transponder was collocated with a permanent Global Positioning System (GPS) antenna at the tide-gauge station IJmuiden (IJMU), see Fig. 3, visible in the descending Radarsat-2 tracks t102 and t202. The transponder was deployed for testing at IJMU in May 2012 (Fig. 1) and imaged from t202. In November 2012, its position was changed for logistical reasons. From August 2013, images from t102 were also made available. Figure 4 shows the temporal performance of radar brightness β_0 at IJMU for both the Radarsat-2 tracks, indicating higher temporal stability after transponder installation.

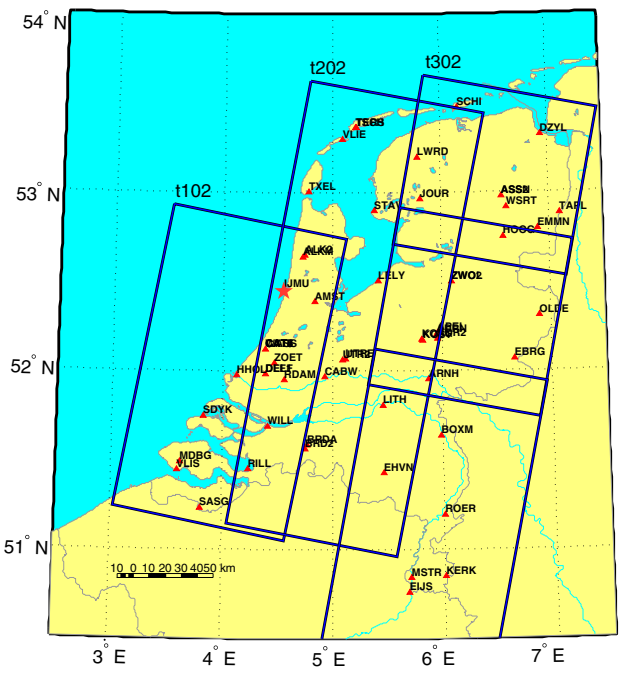

Fig. 3 Location of Dutch permanent GNSS sites and Radarsat-2 tracks. IJMU is marked with a star. Images from track t102 (west) and t202 (centre) have been merged together to form one single long track each

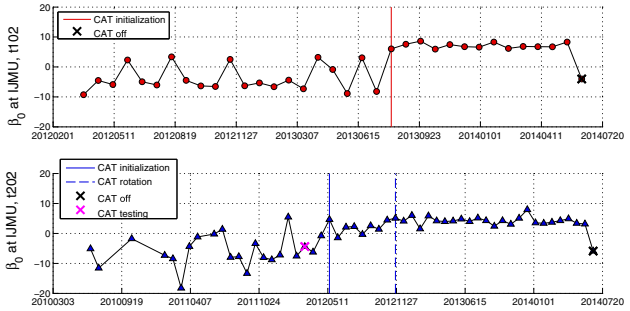

Fig. 4 Time-series of radar brightness (β_0) for the CAT at IJMU using t102 and t202. 'CAT initialization' signifies the first transponding date. 'CAT rotation' indicates adjustment from its initial position to the final one, along the axis of the GNSS antenna pole. 'CAT off' was due to power loss

InSAR displacement analysis of the area around IJMU was performed using Radarsat-2 track t202 and the Delft implementation of the PSI algorithm, DePSI (Kampes 2006; Leijen 2014). The resulting displacement estimates are shown in Fig. 5. The reference point (marked with a white square) is the default chosen by DePSI, based on the temporal coherence estimator, describing the deviation between the observed time-series and the estimated displacement model (Leijen 2014).

In order to determine the 'absolute' displacement of every PS in a TRF, we first refer the PS displacement map to the transponder installed in IJMU, i.e. we make PS #1 the reference point. The GPS-derived displacement at this point is then used as external information on the actual motion of this reference point. An 'absolute' PS displacement map thus results, as shown in Fig. 6.

The IJMU GPS observations are stored in hourly and daily data files, at intervals of 10 and 30 s respectively. These data files in Receiver Independent Exchange (RINEX) format were processed with Bernese 5.0 (Dach et al. 2007) in the high-precision *static mode* with the AGRSCLUS strategy (Huisman 2014) using several European reference frame sites operated by the IGS. The goal was to precisely determine the positions of the antenna in a standard TRF, yielding a time-series of displacements caused by the physical motion of the GPS antenna. The daily and weekly time-series solutions were given in the Solution Independent Exchange (SINEX) format together with the VCM for each solution (Amiri-Simkooei 2007; Bock and Melgar 2016; Williams 2003; Williams et al. 2004; Zhang et al. 1997).

Even a stationary antenna (not undergoing any physical motion) is subject to certain displacements which are not accounted for in a standard TRF. These displacements are very similar for antennas at short distances from each other, and are largely eliminated in a relative setup over short baselines. However, corrections for these displacements are necessary when the baselines involved are up to several hundreds of km (as in our AGRSCLUS case), and are applied in accordance with the conventions specified by the

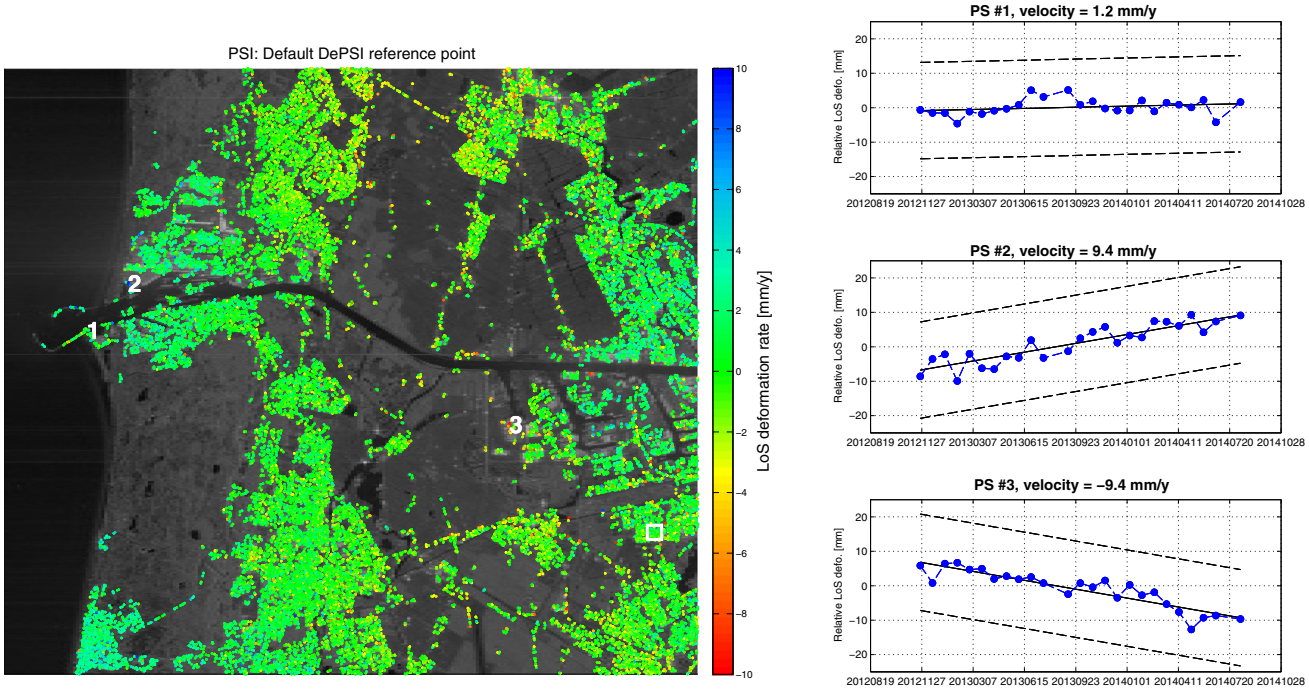

Fig. 5 PS displacement rate map of the IJmuiden area in radar LoS. The default reference point is marked with a *white square*. Three example PS are numbered *1*, *2* and *3*, shown along with their respective displacement time-series (*blue dots*), velocity trends (*black solid lines*) and the uncertainty estimates resulting from phase ambiguity (*black dotted lines*). PS #1 is the transponder installed at IJMU

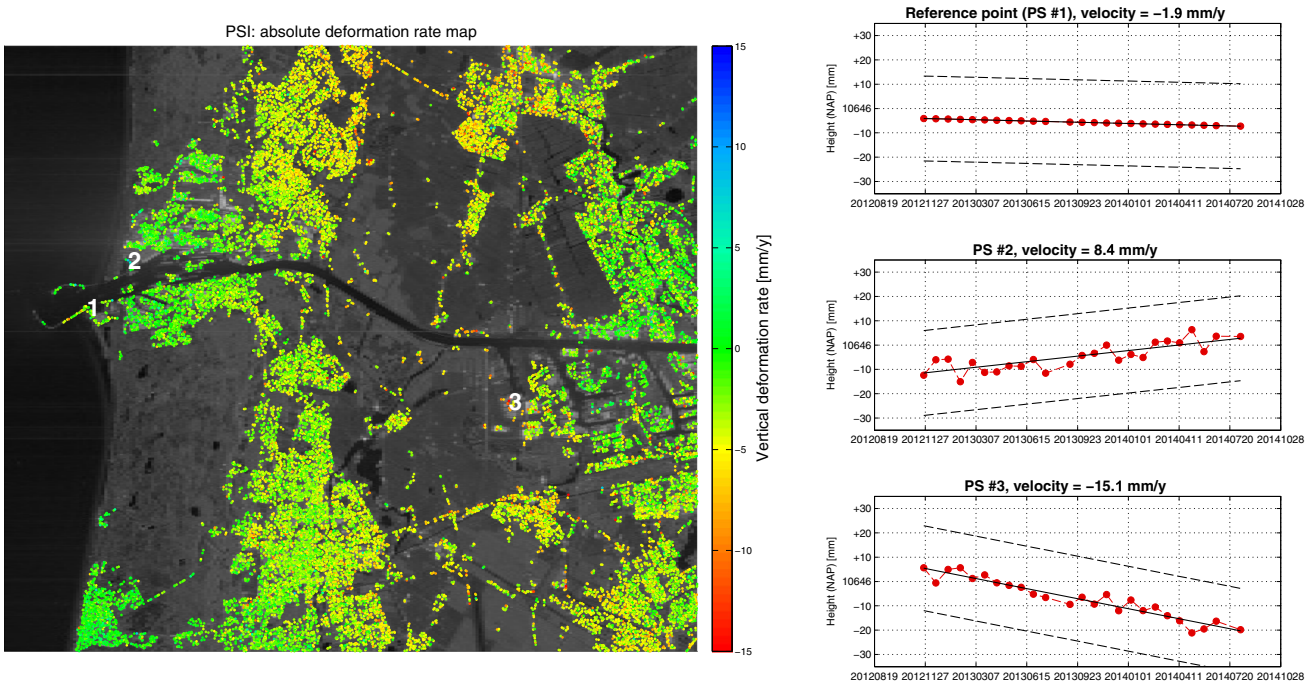

Fig. 6 'Absolute' vertical displacement rate map, referred to the NAP (Amsterdam Ordnance Datum). The time-series are shown as changes in NAP heights (*red dots*). Also shown are the velocity trends (*black solid lines*) and the uncertainty estimates resulting from phase ambiguity (*black dotted lines*)

International Earth Rotation and Reference Systems Service (IERS) (Petit et al. 2016). These include models describing the displacements of the GNSS antenna due to various geophysical effects, such as (Petit et al. 2016) solid earth tides, ocean tidal loading, atmospheric pressure loading, rotational deformation due to polar motion, and other displacements of reference points such as due to environmental conditions. Models used here are, e.g. reference values for local temperature, antenna phase centre offsets and variations, and so on. Non-tidal motions associated with changing environmental loads (very broad spectral content) are not included in the corrections, as they normally change very little over typical integration spans and are less accurately modelled (Petit et al. 2016). Further noise analysis can be performed as in Langbein (2008), Leinen et al. (2013) and Saleh and Becker (2014). The resulting GNSS solutions, (after correction) reflect the physical motion of the station in a standard TRF, even up to the cm- to mm-level.

The corrections specified by the IERS should ideally also be applied to InSAR before datum connection, to be consistent with international conventions. However, given the differential nature of InSAR and the areal extent of a typical SAR image, the effect of these phenomena are expected to largely cancel out; some effects may also leak into the atmospheric phase screen and hence be filtered out, depending on the spatial variation of these signals. For instance, the corrections for solid Earth tides would cancel out, but the effect of ocean loading can be significant. In the Netherlands, we have computed the ocean loading to have amplitudes of 5–17 mm, depending on the location and date. The differential corrections vary between 1 and 3 mm for two nearby GNSS stations inland, to amplitudes between 2 and 5 mm for two tide-gauges at the Dutch coast that are 62 km apart. This effect will be absorbed to a large extent by the atmospheric phase screen, but some residual effects may remain. In case of wide-area InSAR processing (over several hundreds of km), these effects would need to be evaluated prior to datum connection, and if found to be significant, the deformation estimates corrected for Fuhrmann et al. (2015).

The GPS weekly solutions of the IJMU permanent station were converted to orthometric heights by subtracting the local geoid, yielding orthometric heights in the Amsterdam Ordnance Datum *Normaal Amsterdams Peil* (NAP), as shown in Fig. 7. The associated confidence intervals are propagated from the information contained in the SINEX files, scaled based on empirical variance information available for IJMU. The IJMU GPS antenna was replaced in 2014, causing an offset in the time series. A longer time-series of observations with the new antenna is required to reliably estimate this offset. Therefore, we utilized data only from the older GPS antenna in our analysis, i.e. a time-series spanning eight years (2006–2014).

The reference position of the IJMU GPS in metres is known to be $(X, Y, Z) = (3882053.2800, 309346.2071, 5034330.2291)$ in ETRS89/ETRF2000 at epoch 2010.0, which is converted to the RD (*Rijksdriehoekscoördinaten* in

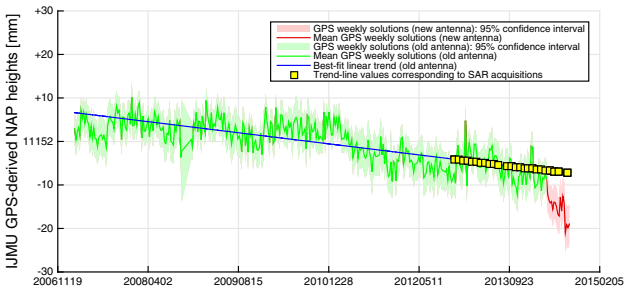

Fig. 7 IJMU GPS time-series (weekly solutions), converted to orthometric height changes in the NAP. The solutions marked in green are used for our analysis; those in *red* have been made after the antenna was replaced at IJMU. The IJMU GPS shows a subsidence rate of 1.9 mm/y, based on the estimated linear trend. The trendline values corresponding to the Radarsat-2 t202 acquisition dates containing the collocated transponder are also displayed in *yellow*

Dutch) and (orthometric) NAP reference frame using standard transformation routines (de Bruijne et al. 2005). Figure 7 therefore shows the GPS solutions (in Up-direction only) as NAP heights. A linear displacement trend is estimated for the time span between 2006 and 2014, i.e. prior to antenna replacement in 2014. This GPS-derived linear trend is used as $v(p_0)$ in Eq. (3) to obtain 'absolute' InSAR displacements.

4.1 Datum connection

The ideal datum connection would be *instantaneous*, i.e. to use the best estimate of the instantaneous position of the GPS antenna at the time of each SAR acquisition. The requirement, however, is that instantaneous GPS position estimates be available with at least the precision achievable with InSAR, i.e. mm-level precision. GPS solutions with the highest precision are achieved using *static* processing, where the computed position is based on GPS observations collected over a length of time, e.g. an hour, a day or a week. This processing strategy eliminates many of the temporal error sources, e.g. due to the atmosphere (estimated), multipath effects (averaged out) and loading mismodeling (averaged out). The precision is therefore a function of the observation duration.

To reach mm-level precision, a minimum observation time of two days is recommended (de Bakker 2016). Instantaneous positions, e.g. computed at a 10- or 30-s interval, are possible; however, these positions have a significantly reduced precision, and are more susceptible to systematic errors and carrier-phase multipath effects (de Bakker 2016). For the IJMU station, 30-s kinematic solutions yield standard deviations of about 2 cm, incompatible with the mm-level InSAR phase precision. Therefore, for precise geodetic datum connection, static GPS processing is inevitable, causing the actual movement of the GPS antenna within the averaging period to smooth out, including any sudden anomalous motion that may occur around the time of the SAR acquisition. We choose to use weekly GPS solutions, which have precision levels comparable to InSAR, i.e. <5 mm (as shown in Fig. 7), with the reasonable assumption of no sudden anomalous or nonlinear displacement of the sturdy and well-founded permanent GPS station within the time span of a week.

Summarizing, there is a trade-off between the precision of GPS observations/solutions and the assumption of displacement signal smoothness; the longer the averaging period, the higher the resulting GPS precision, but the stronger the assumption on displacement signal smoothness.

To perform datum connection in the area of IJmuiden, the InSAR results of the area are referred to the transponder, which then has a postulated time-series with zero displacement. In reality, however, the reference point is also a scatterer, with thermal noise and a certain unknown coherence per epoch, which we term as the *reference point noise* (RPN) (Chang and Hanssen 2016). If not accounted for, the RPN manifests in the time-series of every other PS, in addition to their own noise. RPN removal corrects for anomalous motion that affects only the reference point and not the other PS, as well as biases e.g. due to atmospheric or orbital errors. We isolate and remove the RPN as follows (Chang and Hanssen 2016):

1. *Temporal deramping* The displacement model (e.g. linear rate) of each PS is subtracted from the corresponding displacement time-series. The residues contain noise and any unmodelled displacement.
2. *RPN estimation* The temporally deramped PS are averaged per epoch, and then contain the components present in all the PS at that epoch. We attribute these components to the RPN, shown in Fig. 8c.
3. *RPN removal and reramping* For each PS (except the reference point), the RPN is subtracted from the displacement for all epochs, and the corresponding displacement model is added back to each time-series.

Comparing Fig. 8a, b shows that RPN correction reduces the component of temporal variability of the displacement estimates that appears in all the PS. The RPN is not added back to the reference point, and therefore the remaining motion can then be modelled by the linear displacement derived from the collocated GPS antenna. We estimate a displacement model through the weekly GPS solutions, as shown in Fig. 7. Based on this (linear) model, the IJMU GPS station is found to subside at the rate of 1.9 mm/y. This is then the time-series of the reference point, PS #1, shown in Fig. 6, with the displacement rates of all other PS affected accordingly.

Figure 6 now shows the 'absolute' vertical displacement rate map of the IJmuiden area, referred to a standard TRF

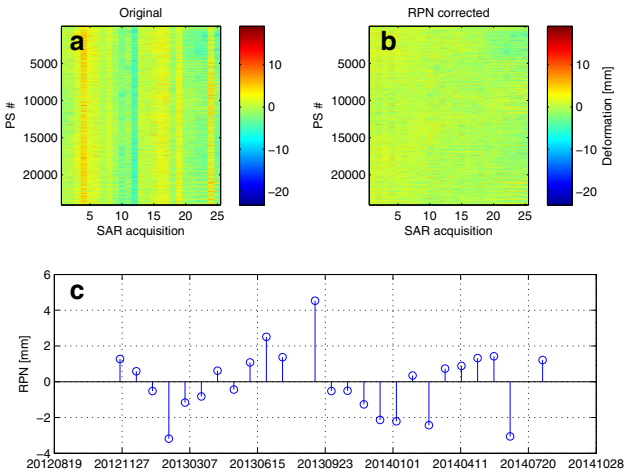

Fig. 8 Plots showing the spatio-temporal variation of displacement **a** before, and **b** after RPN mitigation. Note that RPN correction reduces noise in the temporal direction, which appears as vertical bands in **a**. **c** Estimated RPN per epoch

(ITRF converted to the Dutch national NAP height). The time-series of each PS in this map denotes their variation in NAP heights. Comparing the 'absolute' displacement in Fig. 6 with the default DePSI results of Fig. 5, we observe significantly differing PS displacement rates; in fact, the transponder (i.e. PS #1) shows opposite directions of displacement.

In this case study, we have chosen to project the LoS InSAR displacement estimates to the vertical direction (assuming no horizontal displacement) and use only the Up-component of the GPS solutions for datum connection, so that the resulting displacement map can be defined as changes in (NAP) heights. It is also possible to perform datum connection in the radar LoS direction, by using the 3D GPS solutions projected to the radar LoS. Then the displacement results can be described as changes in (X, Y, Z) coordinates in an earth-centred TRF, instead of (NAP) height changes.

The 'absolute' displacement in Fig. 6 can directly be compared with any other information that is in the RD-NAP system, such as historical leveling data or sea-level changes. As an example, Fig. 9 shows the changes in the sea level as measured by the tide-gauge at IJMU over the last century, referred to the NAP.

5 Additional experimentation

It has been discussed earlier that precise datum connection requires the location of the effective scattering phase centre of the transponder to be known, to ensure that there is no relative displacement between this phase centre and the GNSS antenna. There should ideally be no other dominant radar scatterer (or PS) within the resolution cell of the transponder, since otherwise the effective phase centre (vector sum of

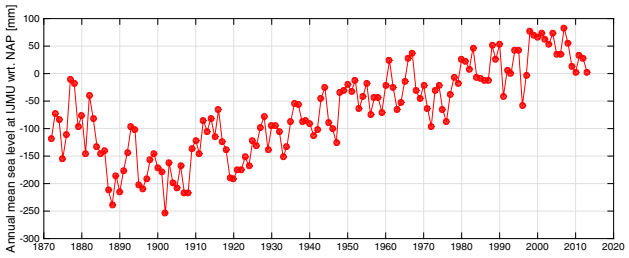

Fig. 9 The annual mean sea level in the period 1872–2013, as measured at the IJmuiden tide-gauge station, referred to the NAP (Holgate et al. 2012; Tide Gauge Data 2015). Such information, in conjunction with a coastal displacement map also referred to the NAP, can be used for flood-risk mapping

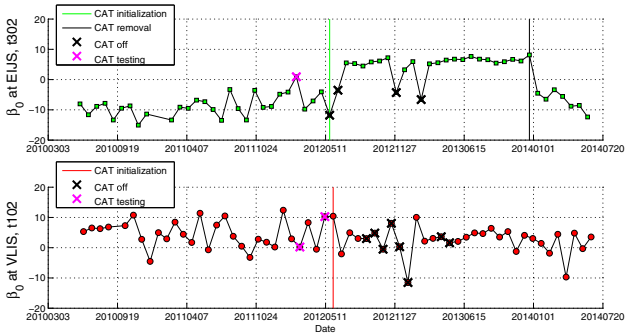

Fig. 10 Time-series of radar brightness (β_0) for the CATs at EIJS and VLIS using t302 and t202, respectively. 'CAT initialization' and 'CAT removal' signify the first and last transponding dates, respectively. 'CAT off' was due to power loss, and 'CAT testing' show dates when visibility tests were performed prior to final installation

the phasors resulting from the transponder and the other scatterer) would once again be unknown. For this reason, good candidate locations for GNSS-augmented transponders are locations that do not already contain PS (Mahapatra et al. 2015), and do not have bright ambient clutter.

In addition to IJMU, transponders were collocated with GPS antennas at two other stations: Eijsden (EIJS) and Vlissingen (VLIS), visible in Fig. 3, respectively, at the south-eastern and southwestern corners of the country. VLIS had high levels of ambient clutter (ships and several metallic structures), EIJS had very low clutter (grassy fields) and IJMU had intermediate clutter levels. The time-series of radar brightness β_0 at EIJS and VLIS are depicted in Fig. 10. During the period that the transponder was operational, EIJS in particular (low ambient clutter, Fig. 11b) shows much smaller variability and much higher average values of β_0. The high ambient clutter at VLIS (Fig. 11c) led to no significant improvement in the phase stability after transponder installation. Based on these experiences, we explore in the following section the feasibility of datum connection at the 52 permanent GNSS stations across the Netherlands.

5.1 Feasibility of transponder collocation at GNSS stations

With the objective of collocating transponders with GNSS antennas at locations with minimum phase interference from other bright radar scatterers, we set out to determine candidate GNSS stations in the Netherlands that are not already PS, and do not contain strong scatterers in the neighbouring pixels.

The locations of the 52 permanent GPS stations investigated in this study are shown in Fig. 3. The automated SAR processing of the three Radarsat-2 tracks (t102, t202 and t302) entailed coregistration and resampling of each slave image to a common grid with that of the master image. Radar coordinates (line and pixel numbers) were computed from the coordinates of the GNSS stations at antenna height. Using the line and pixel numbers, image crops of 300 × 300 m around the GNSS stations were generated. The range coordinates were corrected for atmospheric delays, assuming the same Zenith Total Delay (ZTD) for every day and all stations. Geolocation quality has been verified at three locations with operating transponders; the quality is of the order of 1 pixel (i.e. a few metres).

To determine the suitability of a GNSS site for transponder installation, the following metrics are considered:

– *Radar brightness* (β_0): A site with low β_0 prior to transponder installation is preferred. The empirical threshold on β_0 is based on the lessons learnt from transponder deployment in IJMU, EIJS and VLIS; IJMU was the GNSS station with the maximum β_0 (Fig. 11a) that still showed an improvement when a transponder was installed.

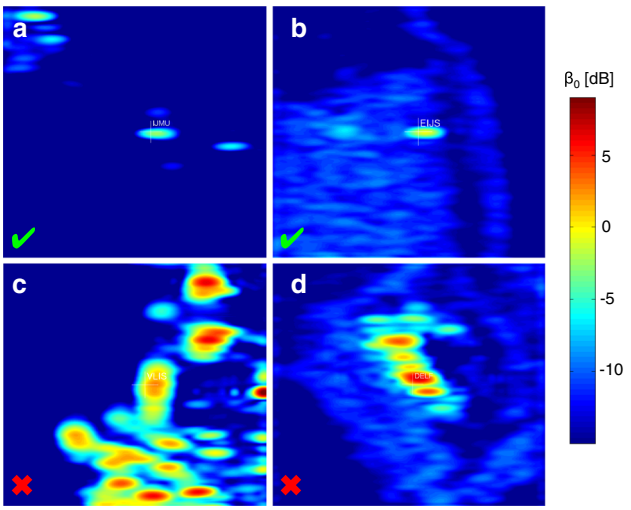

Fig. 11 β_0 characteristics in 300 × 300 m areas around some example GNSS stations, before transponder installation wherever applicable: **a** IJMU, **b** EIJS, **c** VLIS and **d** DELF. Based on the ambient clutter, **a**, **b** are examples of good locations, whereas **c**, **d** are not suitable for collocation with transponders of RCS ∼32 dBm^2, using Radarsat-2 data in the descending mode

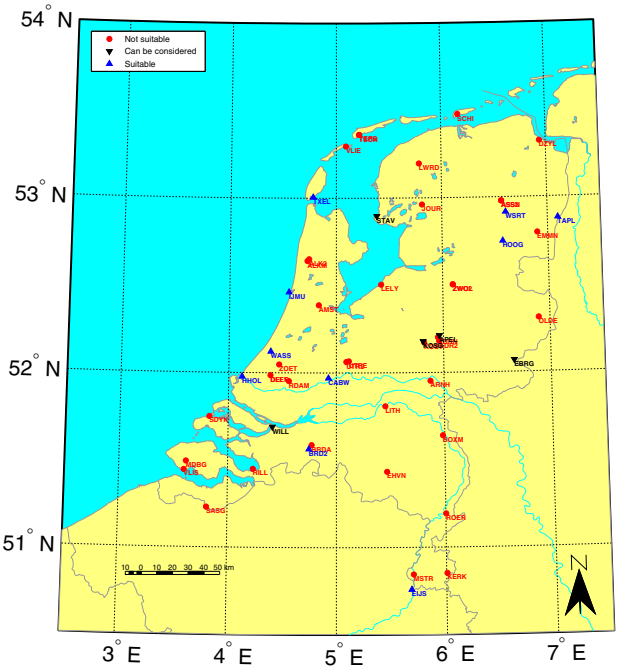

Fig. 12 Map of 52 permanent GNSS stations in the Netherlands, depicting their suitability for collocation with transponders of RCS ∼32 dBm^2, using Radarsat-2 data in the descending mode

– *Signal-to-clutter ratio* (SCR): A relation can be derived between the phase variance and the SCR as Adam et al. (2004)

$$\sigma_\phi^2 = \frac{1}{2 \times \mathrm{SCR}}. \tag{18}$$

Adopting a threshold on the noise level in the phase observations of 0.5 rad, a threshold for the average SCR over all images of 2 dB is obtained; this can be used to detect if a pixel is a candidate PS (Kampes 2006; Leijen 2014) before transponder installation.

The radar backscatter of the GNSS stations was also visually inspected, using mean reflectivity maps (average β_0) and animations of changes in amplitude characteristics at and around GNSS stations. Figure 11 shows the β_0 characteristics around a few example GNSS stations.

Using results both from visual inspection and from thresholding the metrics, we produce a transponder collocation feasibility map of all permanent GNSS stations considered in the Netherlands, shown in Fig. 12. Note that more powerful transponders (with higher RCS) or coded transponders may still be usable at some of the stations that have been marked as unsuitable.

The feasibility map indicates that finding suitable GNSS stations for transponder collocation is not a trivial task. About

Fig. 13 Example of a collocated transponder-GNSS portable installation [I2GPS (Komac et al. 2012, 2015; Mahapatra 2015)] in the Slovenian Alps

70–80% of the stations were found to be unsuitable for transponder collocation, being mounted on buildings which are bright radar scatterers, and in urban areas surrounded by strong levels of clutter. Despite this, each of the three Radarsat-2 tracks in the Netherlands contains more than one suitable GNSS station for datum connection with InSAR. In other parts of the world with less dense networks of permanent GNSS stations, a portable collocated transponder-GNSS installation [I2GPS (Komac et al. 2012, 2015)] can be deployed at locations with low background clutter, as shown in Fig. 13. The position and deformation rate of the GNSS antenna of the I2GPS unit can be determined in a TRF with respect to a reference permanent GNSS station, and used for subsequent datum connection with InSAR via the collocated transponder. Suitability for InSAR datum connection should be considered for future designs of permanent GNSS networks.

6 Conclusions

InSAR time-series in an arbitrary, unknown datum can be efficiently connected to a standard geodetic datum using a collocation between a GNSS antenna and a compact active radar transponder. Given the number of available GNSS reference stations in large parts of the world, in combination with a continuous increase in coverage of SAR acquisitions and the decreasing costs of compact transponders, this paves the way for a standardized approach for the global integration of InSAR results in standard datums, such as the International/European Terrestrial Reference Frame (ITRF/ETRF).

The approach also enables the connection of overlapping or non-overlapping radar datasets, from different viewing geometries or satellite sensors, yielding datasets comparable over large distances, even across oceans and continents. Additionally, region-wide deformation can be linked to sea-level changes via collocated InSAR-GNSS measurements, thereby contributing valuable information in relation to climate change and flood risk.

Further improvements of the proposed approach can be made by increasing the return power of the transponder, which is required in areas of high clutter. Moreover, particularly for unstable GNSS stations, the instantaneous positioning precision of GNSS would need to be improved with one order of magnitude to allow for a direct position estimate at the time of the SAR acquisition.

References

Adam N, Kampes BM, Eineder M (2004) Development of a scientific persistent scatterer system: modifications for mixed ERS/ENVISAT time series, p 9

Adam N, Zhu X, Bamler R (2009) Coherent stacking with TerraSAR-X imagery in urban areas. In: Urban remote sensing event, 2009 Joint. IEEE, pp 1–6

Agram PS, Simons M (2015) A noise model for InSAR time series. J Geophys Res Solid Earth 120(4):2752–2771

Amiri-Simkooei A (2007) Least-squares variance component estimation: theory and GPS applications. Ph.D. thesis, Delft University of Technology

Baarda W (1981) S-transformations and criterion matrices, Publications on Geodesy, New Series, vol 5, 2nd edn. Netherlands Geodetic Commission, Delft

Bock Y, Melgar D (2016) Physical applications of GPS geodesy: a review. Rep Prog Phys 79(10):106801

Bock Y, Wdowinski S, Ferretti A, Novali F, Fumagalli A (2012) Recent subsidence of the Venice Lagoon from continuous GPS and interferometric synthetic aperture radar. Geochem Geophys Geosyst 13(3):Q03023

Bürgmann R, Hilley G, Ferretti A, Novali F (2006) Resolving vertical tectonics in the San Francisco Bay Area from permanent scatterer InSAR and GPS analysis. Geology 34(3):221–224

Chang L, Hanssen RF (2014) Detection of cavity migration and sinkhole risk using radar interferometric time series. Remote Sens Environ 147:56–64

Chang L, Hanssen RF (2016) A probabilistic approach for InSAR time series postprocessing. IEEE Trans Geosci Remote Sens 54(1):421–430. doi:10.1109/TGRS.2015.2459037. http://ieeexplore.ieee.org/xpls/abs_all.jsp?arnumber=7208887&tag=1

Dach R, Hugentobler U, Fridez P, Meindl M et al (2007) Bernese GPS software version 5.0. Astronomical Institute, University of Bern 640

de Bakker PF (2016) On user algorithms for GNSS precise point positioning. Ph.D. thesis, Delft University of Technology

de Bruijne A, van Buren J, Kösters A, van der Marel H (2005) Geodetic reference frames in The Netherlands. Definition and specification of ETRS89, RD and NAP, and their mutual relationships. Netherlands Geodetic Commission, Delft

Delouis B, Giardini D, Lundgren P, Salichon J (2002) Joint inversion of InSAR, GPS, teleseismic, and strong-motion data for the spatial and temporal distribution of earthquake slip: Application to the 1999 Izmit mainshock. Bull Seismol Soc Am 92(1):278–299

Dow J, Neilan R, Rizos C (2009) The international GNSS service in a changing landscape of global navigation satellite systems. J Geodesy 83(3):191–198

Ferretti A, Prati C, Rocca F (2001) Permanent scatterers in SAR interferometry. IEEE Trans Geosci Remote Sens 39(1):8–20

Ferretti A, Savio G, Barzaghi R, Borghi A, Musazzi S, Novali F, Prati C, Rocca F (2007) Submillimeter accuracy of InSAR time series: experimental validation. IEEE Trans Geosci Remote Sens 45(5):1142–1153

Fromberg A (2014) SEA Ltd.: improving space radar instrument performance using precision transponders. https://www.stfc.ac.uk/RALSpace/resources/PDF/AFromberg-SEA_transponders.pdf. Accessed 12 Aug 2014

Fuhrmann T, Cuenca MC, Knöpfler A, van Leijen F, Mayer M, Westerhaus M, Hanssen R, Heck B (2015) Estimation of small surface

displacements in the Upper Rhine Graben area from a combined analysis of PS-InSAR, levelling and GNSS data. Geophys J Int 203(1):614–631
Gernhardt S, Adam N, Eineder M, Bamler R (2010) Potential of very high resolution SAR for persistent scatterer interferometry in urban areas. Ann GIS 16(2):103–111
Hanssen RF (2001) Radar interferometry: data interpretation and error analysis, vol 2. Springer, Berlin
Hanssen RF (2004) Stochastic modeling of time series radar interferometry. In: Geoscience and Remote Sensing Symposium, 2004. IGARSS'04. Proceedings. 2004 IEEE International, vol 4. IEEE, pp 2607–2610
Holgate SJ, Matthews A, Woodworth PL, Rickards LJ, Tamisiea ME, Bradshaw E, Foden PR, Gordon KM, Jevrejeva S, Pugh J (2012) New data systems and products at the permanent service for mean sea level. J Coast Res 29(3):493–504
Hooper A (2006) Persistent scatterer radar interferometry for crustal deformation studies and modeling of volcanic deformation. Ph.D. thesis, Stanford University
Hu J, Ding XL, Li ZW, Zhang L, Zhu JJ, Sun Q, Gao GJ (2016) Vertical and horizontal displacements of Los Angeles from InSAR and GPS time series analysis: resolving tectonic and anthropogenic motions. J Geodyn 99:27–38
Huisman L (2014) AGRS.NL Jaarverslag (Annual Report), Kadaster (Dutch cadastre). Tech. rep
Huygens C (1646) Letter to Marin Mersenne. Correspondence (1646). 'Motus inter corpora relativus tantum est'
International GNSS Service. http://www.igs.org/. Accessed 23 July 2016
Kampes BM (2006) Radar interferometry: persistent scatterer technique. Springer, Dordrecht
Ketelaar VBH (2008) Monitoring surface deformation induced by hydrocarbon production using satellite radar interferometry. Ph.D. thesis, Delft University of Technology
Ketelaar V, Hanssen R (2003) Separation of different deformation regimes using PS-INSAR data. In: Proceedings of FRINGE, pp 1–5
Komac M, Milanič B, Holley R, Mahapatra P, Hanssen R, van der Marel H, Fromberg A (2012) I2GPS—a new approach to 3D surface displacement monitoring. In: Proceedings IPL symposium Kyoto, pp 119–131
Komac M, Holley R, Mahapatra P, van der Marel H, Bavec M (2015) Coupling of GPS/GNSS and radar interferometric data for a 3D surface displacement monitoring of landslides. Landslides 12(2):241–257
Kuang S (1996) Geodetic network analysis and optimal design: concepts and applications. Ann Arbor Press, Chelsea
Langbein J (2008) Noise in GPS displacement measurements from Southern California and Southern Nevada. J Geophys Res Solid Earth 113(B5):1–12
Leinen S, Becker M, Läufer G (2013) Effect of stochastic model fitting on the significance of CORS coordinate time series parameters. J Appl Geodesy 7(1):21–37
Liu S (2012) Satellite radar interferometry: estimation of atmospheric delay. Ph.D. thesis, Delft University of Technology
Mahapatra PS (2015) Geodetic network design for InSAR: application to ground deformation monitoring. Ph.D. thesis, Delft University of Technology
Mahapatra P, Samiei-Esfahany S, van der Marel H, Hanssen R (2014) On the use of transponders as coherent radar targets for SAR interferometry. IEEE Trans Geosci Remote Sens 52(3):1869–1878. doi:10.1109/TGRS.2013.2255881
Mahapatra PS, Samiei-Esfahany S, Hanssen RF (2015) Geodetic network design for InSAR. IEEE Trans Geosci Remote Sens 53(7):3669–3680. doi:10.1109/TGRS.2014.2381598
Marinkovic P, Ketelaar G, van Leijen F, Hanssen R (2007) InSAR quality control: analysis of five years of corner reflector time series. In: Proceedings of Fringe 2007 Workshop (ESA SP-649). Frascati, Italy, pp 26–30
Petit G, Luzum B (2010) IERS conventions. Technical report, ISBN 3-89888-989-6
Pritchard M, Simons M, Rosen P, Hensley S, Webb F (2002) Co-seismic slip from the 1995 July 30 Mw = 8.1 Antofagasta, Chile, earthquake as constrained by InSAR and GPS observations. Geophys J Int 150(2):362–376
Reale D, Fornaro G, Pauciullo A, Zhu X, Bamler R (2011) Tomographic imaging and monitoring of buildings with very high resolution SAR data. IEEE Geosci Remote Sens Lett 8(4):661–665
Rummel R, Teunissen P (1988) Height datum definition, height datum connection and the role of the geodetic boundary value problem. Bull Geod 62:477–498. doi:10.1007/BF02520239
Saleh M, Becker M (2014) A new velocity field from the analysis of the Egyptian Permanent GPS Network (EPGN). Arab J Geosci 7(11):4665–4682
Stevens S (1946) On the theory of scales of measurement. Science 103(2684):677–680. http://www.jstor.org/stable/1671815
Strang G, Borre K (1997) Linear algebra, geodesy, and GPS. Wellesley-Cambridge Press, Wellesley
Teunissen P (1985) Zero order design: generalized inverses, adjustment, the datum problem and *S*-transformations. In: Optimization and design of geodetic networks. Springer, pp 11–55
Tide Gauge Data. http://www.psmsl.org/data/obtaining/stations/32.php. Permanent Service for Mean Sea Level (PSMSL). Accessed 3 Mar 2015
Tosi L, Da Lio C, Strozzi T, Teatini P (2016) Combining L-and X-band SAR interferometry to assess ground displacements in heterogeneous coastal environments: the Po River Delta and Venice Lagoon. Italy. Remote Sens 8(4):308
Usai S, Hanssen R (1997) Long time scale INSAR by means of high coherence features, pp 225–228
van Leijen FJ (2014) Persistent scatterer interferometry based on geodetic estimation theory. NCG, Amersfoort, The Netherlands
Waegel K, Hounam D, Bauer R, Bloetscher H, Zink M, Schwerdt M, Mayr B (1999) An encoding SAR-transponder for target identification. In: Geoscience and remote sensing symposium, 1999. IGARSS'99 proceedings. IEEE 1999 international, vol 1. IEEE, pp 20–22
Williams SDP (2003) The effect of coloured noise on the uncertainties of rates estimated from geodetic time series. J Geodesy 76(9):483–494
Williams SD, Bock Y, Fang P, Jamason P, Nikolaidis RM, Prawirodirdjo L, Miller M, Johnson DJ (2004) Error analysis of continuous GPS position time series. J Geophys Res Solid Earth 109(B3):B03412. doi:10.1029/2003JB002741
Zhang J, Bock Y, Johnson H, Fang P, Williams S, Genrich J, Wdowinski S, Behr J (1997) Southern California permanent GPS geodetic array: error analysis of daily position estimates and site velocities. J Geophys Res Solid Earth 102(B8):18035–18055
Zhu L, Gong H, Li X, Wang R, Chen B, Dai Z, Teatini P (2015) Land subsidence due to groundwater withdrawal in the northern Beijing plain, China. Eng Geol 193:243–255
Zhu XX, Bamler R (2010a) Tomographic SAR inversion by L1-norm regularization–the compressive sensing approach. IEEE Trans Geosci Remote Sens 48(10):3839–3846
Zhu XX, Bamler R (2010b) Very high resolution spaceborne SAR tomography in urban environment. IEEE Trans Geosci Remote Sens 48(12):4296–4308
Zhu XX, Shahzad M (2014) Facade reconstruction using multiview spaceborne TomoSAR point clouds. IEEE Trans Geosci Remote Sens 52(6):3541–3552